Journal of Molecular Graphics and Modelling 28 (2009) 278–286

Contents lists available at ScienceDirect

Journal of Molecular Graphics and Modelling

journal homepage: www.elsevier.com/locate/JMGM

Structure and dynamics of the GH loop of the foot-and-mouth disease virus capsid

Hiroko Azuma, Shigetaka Yoneda *

Graduate School of Science, Kitasato University, Kitasato 1-15-1, Sagamihara-shi, Kanagawa-ken 228-8555, Japan

ARTICLE INFO

Article history:
Received 6 April 2009
Received in revised form 6 August 2009
Accepted 7 August 2009
Available online 15 August 2009

Keywords:
Integrin
Picornavirus
Virion
Rotational symmetry boundary condition
Molecular dynamics simulation
Apthovirus

ABSTRACT

The GH loop of VP1 of the foot-and-mouth disease virus capsid is important because it is a major antigenic site and an integrin recognition site. The GH loop is disordered in all X-ray structures of the capsid except for serotype O under reduced conditions in which the loop lies on the capsid surface. Although the structure of the capsid–integrin complex has not yet been determined, the GH loop is known to protrude from the capsid surface when the capsid is bound with an antigen-binding fragment (Fab). To clarify the structure and dynamics of the GH loop under natural unreduced conditions before binding to integrins or Fab fragments, we performed molecular dynamics simulation of 16.3 ns long under rotational symmetry boundary conditions for the capsid of serotype O using the X-ray structure of the reduced capsid for the initial coordinates. When the disulfide bond at the base of the GH loop was formed by the molecular mutation method, the loop protruded into the surrounding water, as reported for Fab–capsid complexes, and fluctuated like a tentacle. After equilibration, the GH loop overlapped the surface of the capsid but continued to fluctuate, being directed toward a 2-fold axis. The conformational change of the GH loop after formation of the disulfide bond was explained by a model of elastic tube. The side chains of arginine and aspartic acid of the integrin recognition residues (RGD tripeptide) extended in opposite directions, and the residues on the C-terminal side of the RGD tripeptide formed a hydrophobic cluster in close proximity of the arginine residue of the tripeptide.

1. Introduction

The foot-and-mouth disease virus (FMDV) is classified into the *Apthovirus* genus of the *Picornavirus* family and is the causative agent of foot-and-mouth disease [1]. Since the eradication of rinderpest in the early 20th century, foot-and-mouth disease has been the most important disease affecting livestock, and outbreaks of this disease have repeatedly caused damage to the stock-breeding industry around the world. The FMDV capsid is icosahedrally symmetric and comprises 60 protomers, each of which contains four peptide chains (VP1, VP2, VP3 and VP4) [2]. Refined X-ray structures of the capsid have been determined for three FMDV serotypes: O [3–7], C [8] and A [9,10]. Four X-ray structures have been deposited in the Protein Data Bank [11], including 1BBT (serotype O under natural unreduced conditions) [3,12], 1FOD (serotype O under reduced conditions) [5], 1FMD (serotype C) [8] and 1ZBE (serotype A) [10]. The X-ray structure of 1FOD is shown in Fig. 1.

A major immunogenic site on the capsid is the GH loop (residues 134–160) of VP1 (hereafter designated as the GH loop unless the chain is specified). The central part (residues 145–147) of the GH loop has a conserved Arg-Gly-Asp sequence (RGD tripeptide), known as the integrin-binding site [13,14]. Mutation in the GH loop (except for the RGD tripeptide) and in other portions of the capsid can apparently break the integrity of the epitope by direct interactions and far-reaching perturbations that camouflage the vital residues from antibody attack [2,3,8]. Because the GH loop is extremely mobile, it appears disordered in all X-ray structures except for 1FOD. Serotype O has a cysteine residue Cys134 on VP1 at the base of the GH loop that binds to another residue Cys130 on VP2 via a disulfide bond. When the disulfide bond is formed, the GH loop is disordered and the conformational state is called the 'up' state [4]. When the disulfide bond is broken under reduced conditions by soaking the virus crystal in dithiothreitol before X-ray data collection, the GH loop adopts an ordered conformational state called the 'down' state, whereby it overlaps the capsid surface (Fig. 1) [5]. The RGD tripeptide has an open turn conformation, followed by the residues on the C-terminal side in a helical conformation. The infectivity of the virus is weakened under reduced conditions but not completely lost. Because FMDV virions of serotype O are initially produced in the reduced state, the GH loop is presumably ordered [2]. Oxidation of the mature and disordered form occurs after it is released from the host cell, following which serotype O demonstrates stronger specificity to

* Corresponding author. Tel.: +81 42 778 9404; fax: +81 42 778 9404.
E-mail address: syoneda@kitasato-u.ac.jp (S. Yoneda).

1093-3263/$ – see front matter © 2009 Elsevier Inc. All rights reserved.
doi:10.1016/j.jmgm.2009.08.006

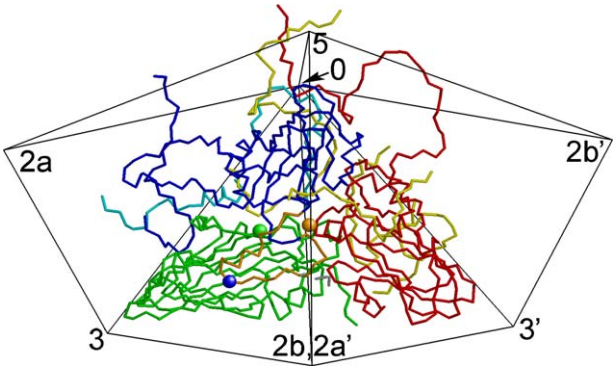

Fig. 1. Asymmetric unit structure of 1FOD seen from the outer surface. The quadrangular pyramid with the vertices labelled 5, 3, 2a, 2b and 0 is the asymmetric unit of icosahedral symmetry used for the computational cell under RSBC (rotational symmetry boundary conditions). Zero (0) is the centre of icosahedral symmetry. The lines from 0 to 5 and from 0 to 3 are 5-fold and 3-fold symmetry axes, respectively. The lines from 0 to 2a and from 0 to 2b represent two 2-fold symmetry axes. The backbones of the polypeptide chains are coloured as follows: VP1, blue; VP2, green; VP3, red and VP4, cyan. VP3 is taken from a 5-fold-related protomer. The GH loop of VP1 is shown in orange. The N- and C-termini of VP1, the C-terminus of VP4 from a neighbouring asymmetric unit and the N-terminus of VP3 from another neighbouring asymmetric unit intrude into the pyramid and are depicted in yellow. The blue sphere depicts the C_α atom of Gly146 on VP1. The green and orange spheres depict the S_γ atoms of Cys134 on VP2 and Cys130 on VP1, respectively. Because some residues of the 1FOD structure are out of the computational cell, a neighbouring asymmetric unit (quadrangular pyramid of 5, 3′, 2a′, 2b′ and 0) is also shown.

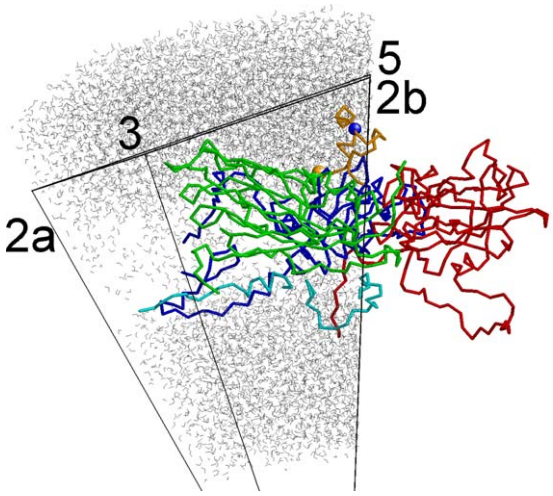

Fig. 2. Side view of the simulation structure at 16.3 ns. The colours of the polypeptide chains are the same as those in Fig. 1. Water molecules are grey. Some residues are shown outside the computational cell, but these were calculated correctly in the cell under RSBC.

the integrin. For other serotypes, there are no corresponding cysteine pairs. All the X-ray structures of other serotypes are in the up state and thus their GH loops are disordered.

In addition, X-ray analysis has been performed on the complexes of the Fab fragments of neutralizing monoclonal antibodies and the synthetic peptides representing the GH loop [15–18]. Assessment of the X-ray structure of the Fab–peptide complex combined with cryoelectron microscopy, used for visualization of binding between the capsid and Fab fragments, has shown that the GH loop protrudes outward from the surface in the capsid–Fab complex [19,20]. No similar studies have been conducted for the capsid–integrin complex. However, the protruding conformation of the GH loop is assumed to be similar. High-resolution X-ray structures have been determined for the extracellular segments of integrins in the unligated state and in complex with high-affinity ligands [21–23]. These analyses present conformation of the RGD tripeptide after binding to integrin. However, the conformation and dynamics of the GH loop before binding are as important as those after binding because binding of molecules is governed by the free energy difference between before and after binding. In the present study, the conformation and dynamics of the GH loop before binding to integrin were ascertained by molecular dynamics (MD) simulation using 1FOD for the initial coordinates.

Considering the large size of the GH loop, we performed MD simulation of the entire capsid under rotational symmetry boundary conditions (RSBC) [24–26]. RSBC is used to restrict the calculations required for an icosahedrally symmetric capsid to one asymmetric unit, including its interactions with neighbouring asymmetric units. Theoretically, simulation under RSBC is at least 60 times faster than simulation of an entire asymmetric capsid, though such extensive simulations are becoming more practical these days [27]. RSBC has already been applied to simulation of the rhinovirus capsid [25,28] and to structure prediction of the poliovirus capsid from the structure of the rhinovirus capsid [29]. It has also been applied to simulation of a glycogen phosphorylase crystal in $P4_32_12$ symmetry [30]. In the present study, MD simulation was performed using the structure of serotype O under reduced conditions (1FOD) for the initial coordinates. The molecular mutation method [31,32] was used to form the disulfide bond between Cys134 on VP1 and Cys130 on VP2. Therefore, the simulated structure obtained after molecular mutation can be considered to be that of an unreduced capsid, which should equal the structure of 1BBT except for the disordered regions that include the GH loop. Thus, MD simulation could be used to analyse the structure and dynamics of the GH loop under natural unreduced conditions.

2. Materials and methods

Protonation of histidine residues was determined by considering electrostatic potentials and hydrogen-bonding networks involving the neighbouring residues. The N- and C-termini that

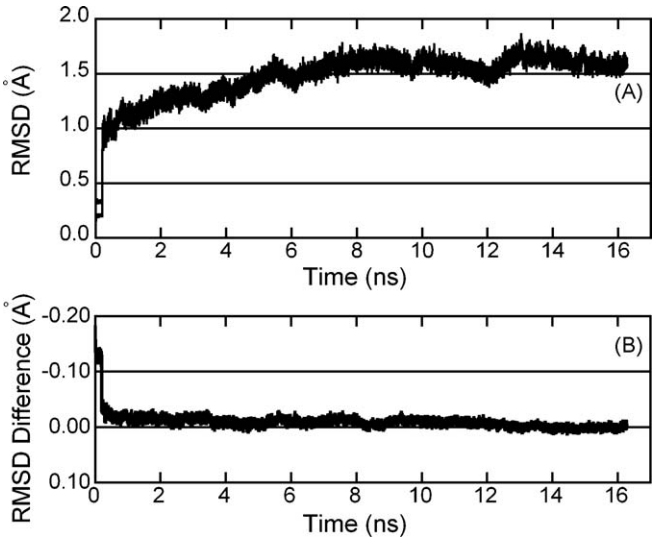

Fig. 3. Time profiles of RMSD of the simulation structure from the 1FOD and 1BBT structures. The RMSD values were calculated for the C_α atoms that have the experimental B-factors smaller than 10 Å^2 in both 1FOD and 1BBT. (A) The RMSD from 1FOD overlapped that from 1BBT at the almost same positions. The curves gradually increase to about 1.7 Å. (B) The RMSD difference (the RMSD from 1BBT subtracted by that from 1FOD) is shown. Initially the difference was 0.15 Å and the simulation structure was closer to 1FOD than 1BBT. During the final 1 ns, the average of the difference was −0.01 Å.

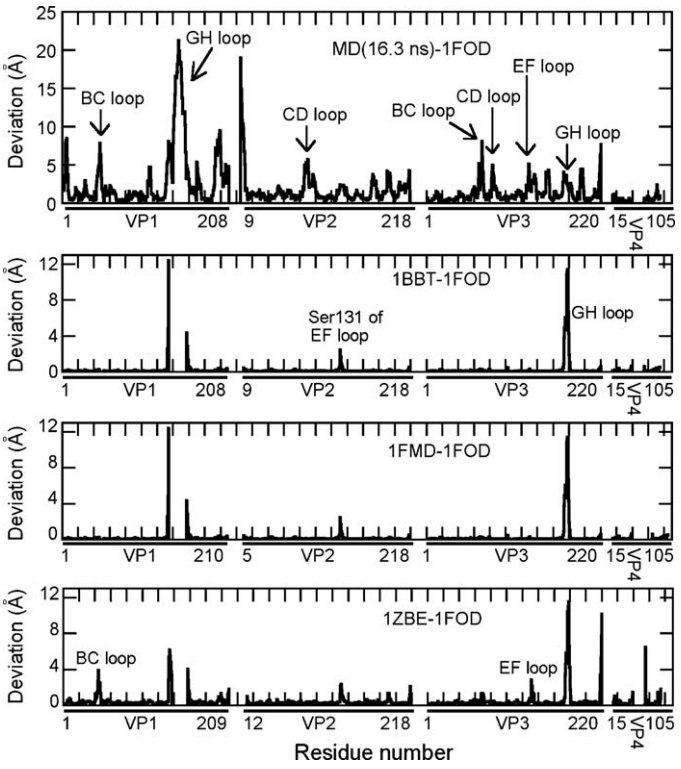

Fig. 4. Deviations of the C_α atoms of the 16.3-ns simulation structure from 1FOD. The abscissa shows the residue numbers for 1FOD. The deviations of 1BBT, 1FMD and 1ZBE from 1FOD are also shown for comparison. Ser131 on VP2 is a neighbour of Cys130 on VP2 that forms a disulfide bond with Cys134 on VP1. In 1FOD, this disulfide bond is broken, but it forms in 1BBT. The other serotypes (1FMD and 1ZBE) have no cysteines corresponding to Cys130 on VP2. The BC loop of VP1 contains many residue mutations in 1ZBE, and the EF loop of VP3 has a residue insertion in 1ZBE.

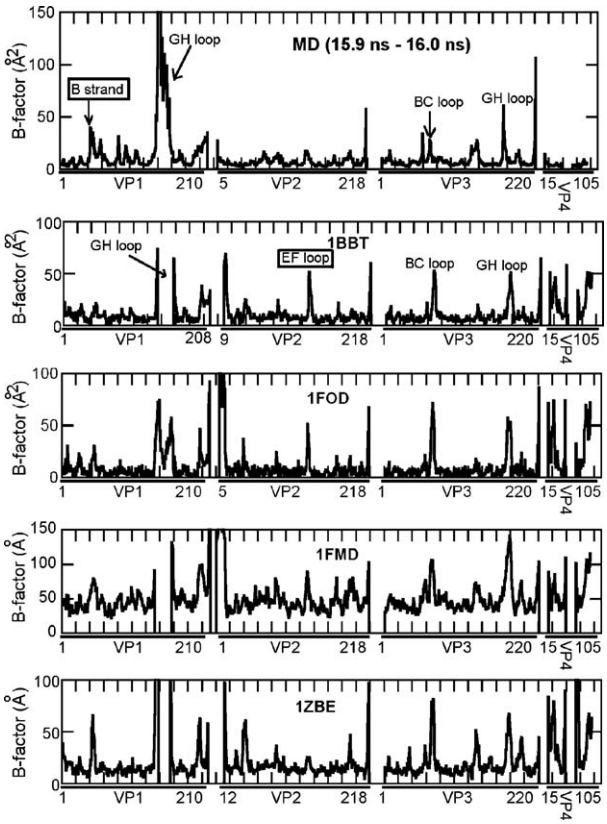

Fig. 5. B-factors of the C_α atoms from simulation. The experimental B-factors are also shown for comparison. Extremely large B-factors are not shown because of the likelihood of experimental and simulation errors. The maximum B-factor obtained by the simulation is 301 Å^2 at Pro142 of VP1. The scale of the ordinate is different for 1FMD. The simulated B-factors were calculated as $B = (8\pi^2/3)\langle(\Delta x)^2\rangle$, where Δx is the positional fluctuation of an atom and $\langle\rangle$ denotes the time average. The labels of positions of the B strand of VP1 and the EF loop of VP2 are enclosed by rectangles.

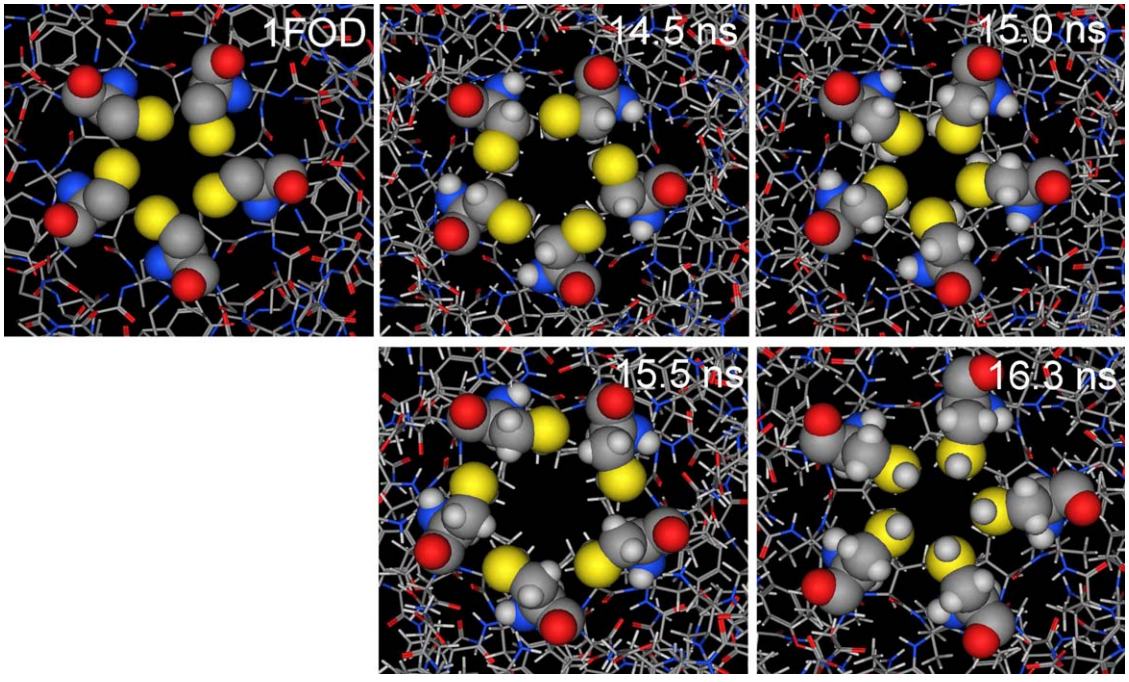

Fig. 6. Structure of the 5-fold annulus as viewed from the exterior of the capsid. All the atoms of the symmetry-related neighbouring protomers near the 5-fold axis are shown. The atoms of Cys7 on VP3 are shown as spacefill models. The motion of the annulus was not influenced by the positional constraints because Cys7 on VP3 is not close to the inner surface and is separated from the constrained atoms by 13 Å in Cartesian space and by 17 residues in the VP3 sequence. The orientation of the side chain was the same as that in 1FOD at 15.5 ns, but it fluctuated and was in a direction opposite to the orientation in 1FOD at 14.5 ns. The S_γ atoms were directed toward the 5-fold axis at 15.0 ns and 16.3 ns, but the direction of H_γ at 15.0 ns was opposite to the direction of H_γ at 16.3 ns.

were truncated by disorder received additional acetyl (ACE) and N-methyl (NME) residues, respectively, of the AMBER energy parameters [33,34]. The ordinal N- and C-termini of the chains were assumed to be charged. The inner and outer radii of the capsid from the centre of icosahedral symmetry were 99.4 Å and 153.0 Å, respectively, and the region with radius ranging from 69.5 Å to 177.5 Å was filled with water molecules, as shown in Fig. 2. A half-harmonic potential with a Hooke's constant of 2.0 kcal/(mol Å) was added to the water molecules that were escaping through the inner or outer surface of the water region [25,28]. The region was large enough to encompass the larger movements of the GH loop. We used the APRICOT program to execute MD simulation [25,32]. In addition, we used the AMBER FF03 energy parameters [34] for proteins and the TIP3P potential [35] for the surrounding water. A dielectric constant of 1 and a cut-off of 18 Å were used. Initially, energy minimization was performed under RSBC with positional constraints on all the protein atoms determined by X-ray analysis. Thus the positions of other atoms including water, hydrogen, and disordered atoms were optimized. Subsequently, using the leap-frog method [36], the SHAKE method [36,37] and a 2-fs time step, we performed MD simulation with the same positional constraints under RSBC. The initial velocity was generated by a random function having the Boltzmann distribution with temperature of 300 K. By the principle of energy equipartition between the potential energy and the kinetic energy, temperature decreased to about 50 K, when the simulation proceeded for 0.5 ps. In order to keep temperature to be constant, we adopted the velocity-scaling method which does not produce a rigorous canonical ensemble, but is widely used for computational simplicity [36,38]. Initially, the parameter of 'relaxation time' for the velocity-scaling method was 10 ps, and temperature gradually increased to about 300 K. After 50 ps, the parameter was changed to 0.5 ps to more strictly keep temperature to be 300 K. The average of temperature was 304 K and its root mean square deviation was 1.2 K after 50 ps. After 0.2 ns, we executed further MD simulation without the above positional constraints until 16.3 ns. Because the FMDV capsid is thinner than those of other picornaviruses, shrinkage of its radius [25,26,28] was larger in our preliminary simulations (data not shown). Thus, we added other positional constraints with a Hooke's constant of 2 kcal/(mol Å) to 121 atoms that were selected on the inner surface of the capsid. The distance of all these atoms from the centre of icosahedral symmetry was less than 122 Å, and 80 of them were in VP4. The disulfide bond between Cys134 on VP1 and Cys130 on VP2 was formed by the molecular mutation method using the coupling parameter approach [31,32], when the simulation proceeded about 1 ns; i.e., the molecular mutation was performed between 0.900 ns and 0.985 ns. From preliminary simulations, the conformation of the GH loop after mutation is not

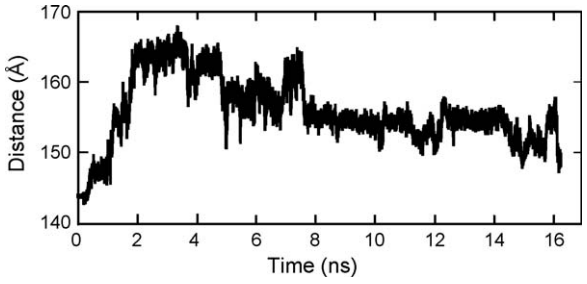

Fig. 7. Time profile of the distance of the centre of the RGD tripeptide from the origin (the centre of icosahedral symmetry). From 7 ns to 12 ns, the torsion angle between the S_γ atoms of Cys134 on VP1 and Cys130 on VP2 rotated by approximately −540° from −90° to +90°. This rotation was correlated with the rotation of the neighbouring torsion angle between C_β and S_γ of Cys134 on VP1 by +360° from +60° to +60° and the rotation of the torsion angle between S_γ and C_β of Cys130 of VP2 by −360° from 180° to 180°.

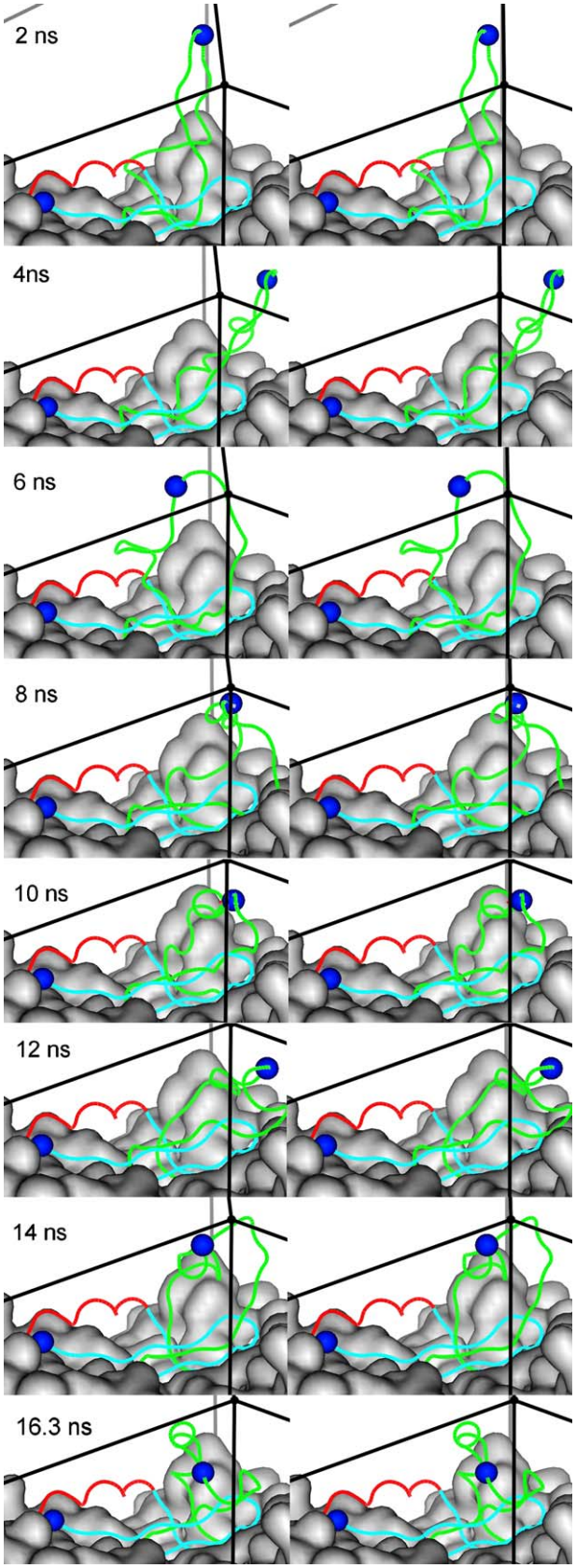

Fig. 8. Structures of the GH loop overlapped the capsid surface at 16.3 ns. Water molecules are not shown. The green tubes depict the GH-loop structure at 2 ns, 4 ns, 6 ns, 8 ns, 10 ns, 12 ns, 14 ns, and 16.3 ns. The initial GH-loop structure is shown as a cyan tube. Red denotes helix.

dependent on the time length of the simulation before the mutation, if the length is longer than a few hundred ps (data not shown). Reflecting the mutation of residues Cys134 on VP1 and Cys130 on VP2 during reduction of cystine to cysteine, the number of atoms (including water) changed from 33 952 to 33 950 after the disulfide bond was formed. The X-ray structure shows a five-stranded β-annulus formed by the N-termini of VP3 packing around the icosahedral 5-fold axes. The five Cys7 residues on VP3 in the annulus are believed to form disulfide bridges under ordinary solution conditions [3]. However, because the disulfide bonds among these five cysteine residues break the 5-fold symmetry, MD simulation assumed that there were no bonds among Cys7 on VP3.

3. Results

Fig. 3 shows the root mean square deviation (RMSD) of the MD simulation structure from the 1FOD X-ray structure. RMSD gradually increased during simulation until it reached a plateau at about 1.7 Å. When the unreduced structure of 1BBT was used to supply the standard coordinates, RMSD was initially about 0.15 Å larger than that obtained from 1FOD and eventually became about 0.01 Å smaller than that obtained from 1FOD. Therefore, capsid mutation from the reduced form to the unreduced form was correctly reflected in RMSD. Fig. 2 shows the final structure of simulation, including the surrounding water. Fig. 4 shows the deviation of each C_α atom of the final structure from 1FOD. There are numerous peaks and valleys in MD(16.3 ns)–1FOD. In contrast, there are almost no deviations in 1BBT–1FOD, 1FMD–1FOD and 1ZBE–1FOD, except for a limited number of peaks and disorders. This good similarity among the X-ray structures may be due to the molecular replacement method, by which the results of the previously determined of X-ray analysis, 1FOD, were used for the determination of phase of X-ray diffraction in the proceeding X-ray analyses, 1BBT, 1FMD and 1ZBE. Because MD simulation is not affected by the molecular replacement method, much more various peaks of deviations are shown in MD(16.3 ns)–1FOD of Fig. 4. As shown in Fig. 5, the B-factors of VP4 are small in MD simulation when compared with the experimental data, because of the positional constraints. The GH loop of VP1 and some terminals of chains had very large B-factors or were disordered in both experimental and simulation studies. The B-factors of the BC and GH loops of VP3 were also large in both experimental and simulation data. The B-factors of the EF loop of VP2 were large in all the experiments except for 1ZBE, but they were not clarified in MD simulation or 1ZBE. Conversely, the B-factors of the B strand of VP1 were small in all the experiments except for 1ZBE, whereas the B strand showed a clear peak in MD simulation and 1ZBE. Thus, considering both the deviations and B-factors in Figs. 4 and 5, the most recent X-ray analysis of 1ZBE rather than 1BBT was the closest to the results of MD simulation.

Fig. 6 illustrates the five-stranded β-annulus that formed around the 5-fold axis. Although the five Cys7 residues on VP3 are believed to form disulfide bonds [3], these bonds were not considered during simulation (as described in Section 2). Therefore, the distance between S_γ atoms was no shorter than 3 Å because of steric hindrance. The average distance between the neighbouring S_γ atoms was 4.2 Å with a standard deviation of 0.7 Å. Although a distance of more than 6 Å between S_γ atoms is uncommon, the longest distance was about 10 Å at about 7 ns.

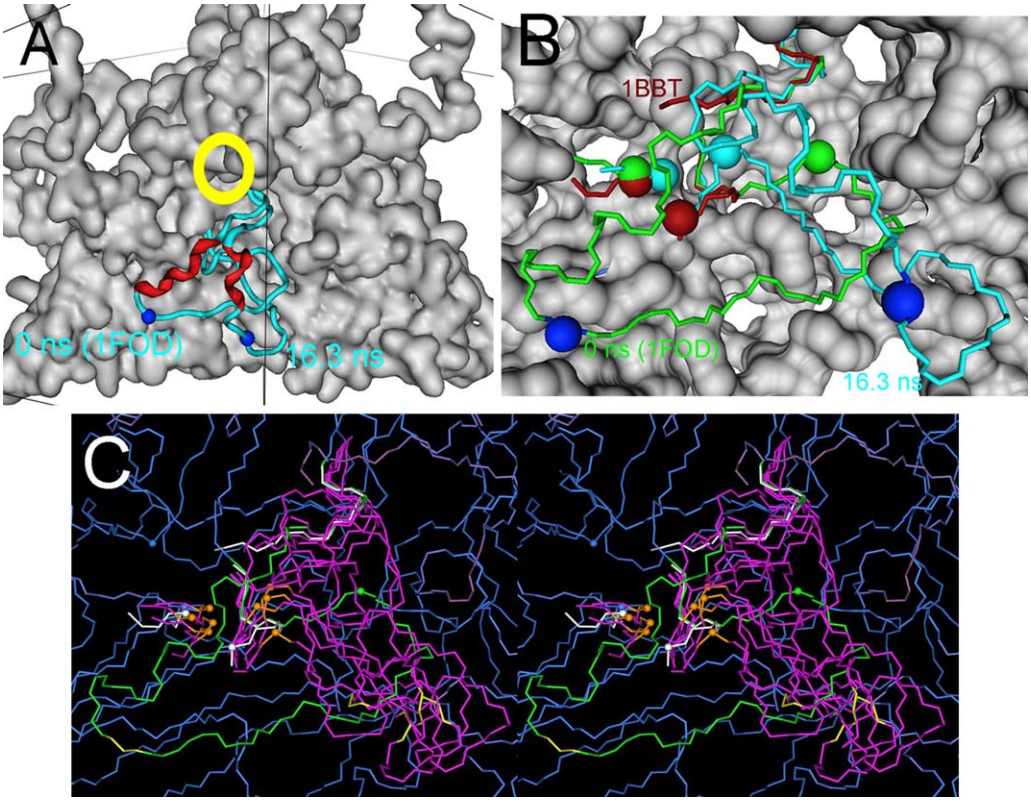

Fig. 9. Initial (1FOD) and final (16.3 ns) structures of the GH loop overlapped the capsid surface at 16.3 ns. (A) View from the outer surface of the capsid, as shown in Fig. 1. The yellow ring depicts the position of the GH loop in the conventional 'up' state [4]. The helical secondary structures are shown in red, and other parts of the GH loop are in cyan. (B) Magnification of (A). The initial and final structures of the GH loop are shown in green and cyan, respectively. The ordered residues at the base of the GH loop in 1BBT are also shown in red. Cys130 on VP2 and its neighbouring residue are also shown. The blue spheres depict the C_α atoms of Gly145 on VP1, and the remaining coloured spheres depict the S_γ atoms of Cys134 on VP1 and Cys130 on VP2. (C) Stereo view of the fluctuating conformational state of the GH loop. The structures at 10 ns, 12 ns, 14 ns, and 16 ns are shown in magenta. Only the N, C_α, and C atoms are shown. The 1FOD structure of the GH loop is shown in green. Gly146 of the RGD tripeptide is yellow. Cys134 on VP1 and Cys130 on VP2 that form the disulfide bond are orange and their C_α atoms are depicted as a ball. The ordered atoms at the base of the GH loop in 1BBT are shown in white.

Despite neglecting the disulfide bond, Cys7 on VP3 did not move far from its position in the X-ray structure. Thus, the disulfide bonds did not stabilize the 5-fold annulus but fluctuated within the stable structure of the annulus, and this stability supported the fidelity of MD simulation.

The time profile of distance of the RGD tripeptide from the centre of the entire capsid (the origin) is shown in Fig. 7. After formation of the disulfide bond at about 1 ns, the distance from the centre rapidly increased. Thus the GH loop rose from the down state and protruded into the surrounding water. It moved like a tentacle as shown in Fig. 8. Later, the GH loop came closer to the capsid surface, as indicated by the gradual decrease of the distance from the centre. Even after the distance converged to about 155 Å in Fig. 7, the GH loop continued to fluctuate as shown in Fig. 9C. The conformational state of the GH loop after 10 ns is composed of a set of fluctuating and equilibrated conformations, which are directed toward one of the 2-fold axis. The motion of the GH loop is not the simple hinge motion of a rigid body. The initial (1FOD) and the final structure are also shown in Fig. 9. After formation of the disulfide bond, the C_α atom of Cys130 on VP2 moves toward Cys134 on VP1 by 1 Å or 2 Å from the initial 1FOD position. The C_α atom of Cys134 on VP1 also moves by 8 Å or 9 Å. The direction of movement of the C_α atoms of Cys134 on VP1 and Cys130 on VP2 is approximately along a line that connects the initial positions of the two atoms. The residues on the N-terminal side of the GH loop near Cys134 are shifted from the initial position for creating a turn conformation to allow formation of a disulfide bond at the base of the loop. Time profile of the secondary structure in Fig. 10 shows conformational transitions of the GH loop during 16.3 ns. By formation of the disulfide bond, turn conformation appeared near Cys134. The secondary structure after 10 ns was also fluctuating, but presenting a set of loop conformations with the C-terminal side of the RGD tripeptide in a helical or turn conformation as in 1FOD.

The backbone conformations of the RGD tripeptide and its two flanking residues are in the helix and turn regions of the Ramachandran plot as shown in Fig. 11. The extended conformation is also shown for the RGD tripeptide, especially for Gly146. Thus both the extended and kink conformations appeared for the backbone of the tripeptide in the simulation. The side chains of

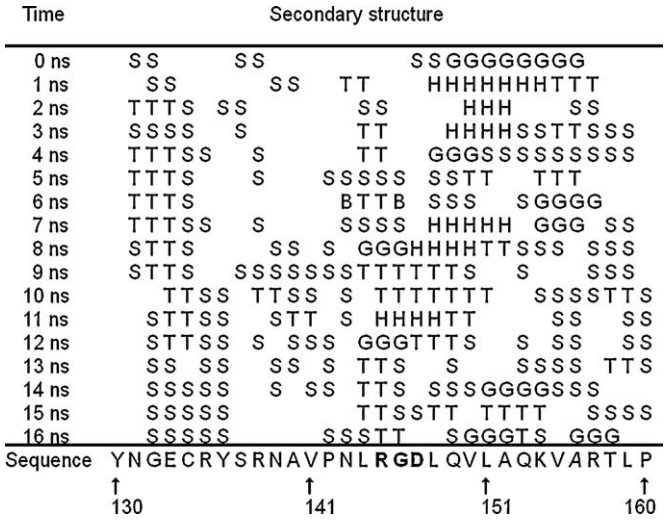

Fig. 10. Secondary structure of residues, including the GH loop. The bottom lines show the residue numbers and the single-letter codes of amino acids in VP1. The secondary structures denoted by H, G, S and T are α-helix, 3_{10}-helix, bend and hydrogen-bonded turn, respectively. The secondary structures were determined with the DSSP program [39] using the Swiss Model web server [40].

Arg145 and Asp147 point in opposite directions, as shown in Fig. 12, and the entire structure of the RGD tripeptide is like a bar with an electrostatic dipole. The residues formed a hydrophobic cluster on the C-terminal side of the RGD tripeptide. The hydrophobic cluster continued to form during MD simulation. Atomic distances among the C_α, C_β and C_γ atoms are often used to analyse conformation of integrin-binding peptides [23]. The distance between the C_α atoms of Arg145 and Asp147 was 6.3 Å with a standard deviation of about 1 Å during the final 2 ns of MD simulation. The distance between the C_β atoms of the residues was 7.8 Å and the distance between the C_γ atoms was 10.0 Å. These distances are similar to the 7.1 Å, 9.1 Å and 11.6 Å distance data in 1FOD, respectively, and are closer to the 6.4 Å, 8.9 Å and 11.5 Å distance data obtained from the cyclic peptide in the integrin–ligand complex (1L5G) [23]. Fig. 13 shows the profiles of RMSD of

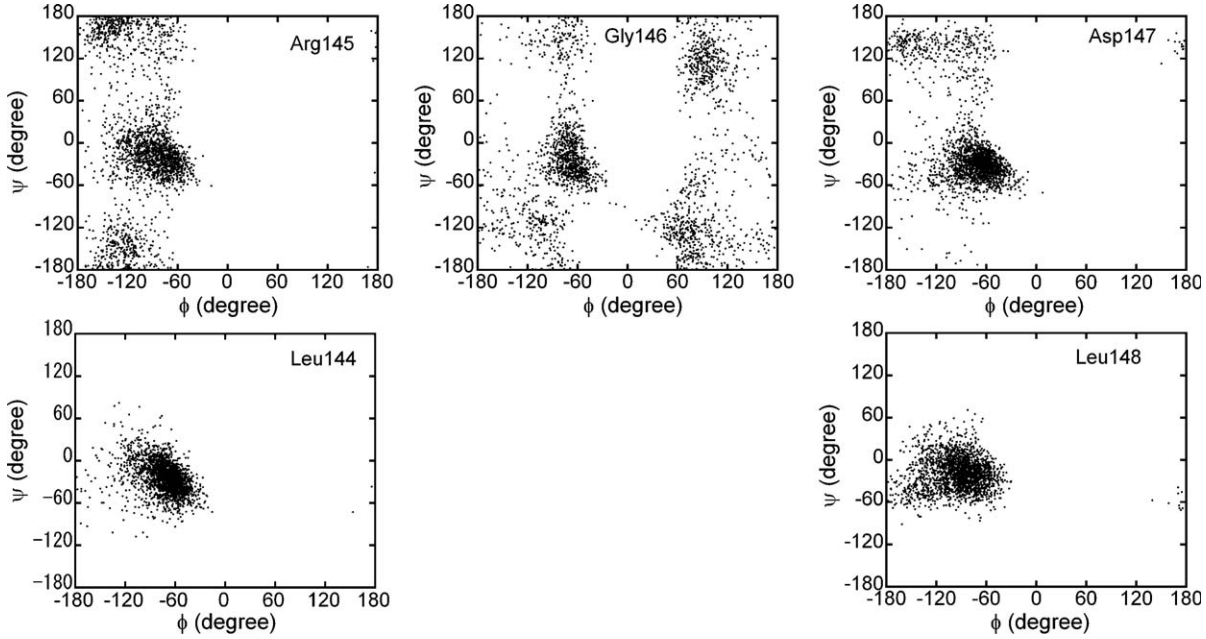

Fig. 11. Ramachandran plot of residues 144–148 on VP1. Data at 1-ps interval during the final 2 ns are plotted.

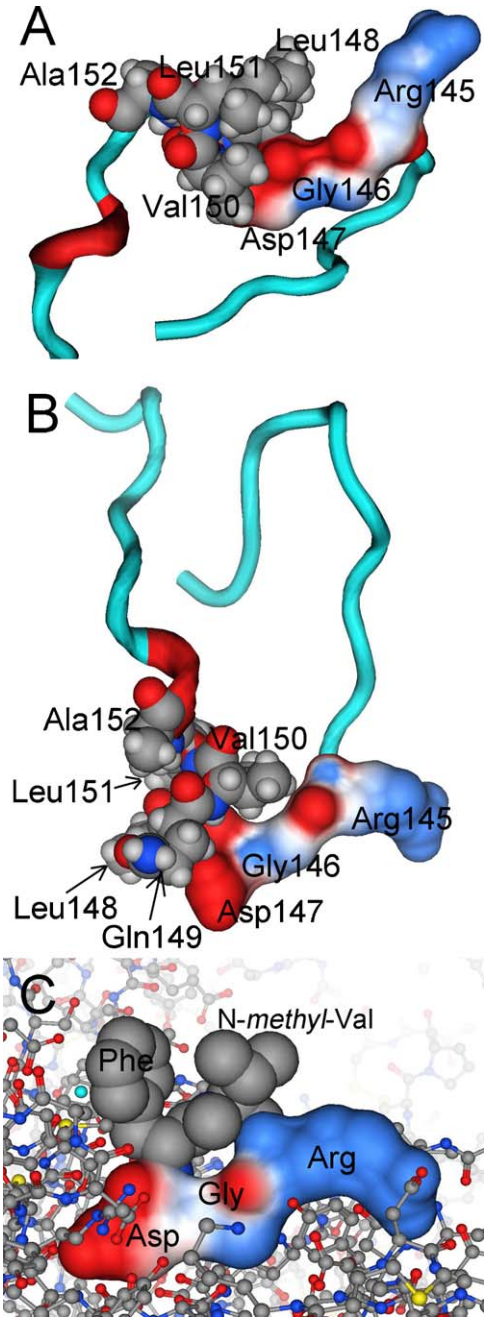

Fig. 12. Conformation of the RGD tripeptide. The five residues on the C-terminal side (Leu148, Gln149, Val150, Leu151 and Ala152) are shown by the sphere models. The RGD tripeptide is shown by Connolly's surface. The blue and red colours depict the positive and negative electrostatic potentials, respectively. The molecules are rotated to show the RGD tripeptides in similar orientations. (A) Structure at 16.3 ns. Gln149 is hidden by other atoms. (B) Initial structure (1FOD). (C) Structure of RGD-containing cyclic peptides in the complex with integrin αvβ3 (1L5G) [23]. The ligand atoms except for the RGD tripeptide are shown by the sphere models, and those of integrin are shown by the ball-and-stick models.

the RGD tripeptide from 1FOD and from 1L5G. The structure of the RGD tripeptide in the simulation is closer to the ligand structure in 1L5G than in 1FOD. The conformations that are very similar to 1L5G with RMSD smaller than 0.5 Å appeared with probability of 0.07 for the final 2 ns. The distance between the C_β atoms of Asp147 of the RGD tripeptide and Leu151 of the hydrophobic cluster was often longer than 12 Å when the GH loop fluctuated like a tentacle, but it was shorter (about 6 Å) in the initial structure and after 12 ns.

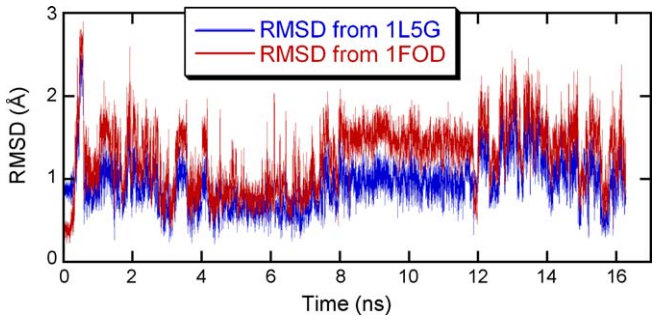

Fig. 13. Time profile of RMSD of the simulation structure of the RGD tripeptide from the X-ray structure of the high-affinity ligand in the ligand–integrin (αvβ3) complex (1L5G) [23]. Time profile of RMSD from 1FOD is also shown. Only the C_α, C_β and C_γ atoms of the RGD tripeptide are considered for the RMSD.

4. Discussion

Our MD simulation revealed that the GH loop rose from the down state and protruded into the surrounding water after formation of the disulfide bond (Figs. 7 and 8). The GH loop then moved like a tentacle for some time. This flexible, protruding conformation is consistent with that shown by investigation of the Fab complexes [19,20]. The GH loop moved closer to the surface of the capsid after equilibration, but it continued to fluctuate (Figs. 8 and 9). Thus, MD simulation showed the following three conformational states of the GH loop:

(1) the down state whereby the GH loop is ordered on the capsid surface and is directed toward the 3-fold axis;
(2) the flexible and protruding conformation, like a tentacle, as found in the Fab–capsid complexes;
(3) the modified up state whereby the GH loop fluctuates and is directed toward one of the 2-fold axes.

The conformational state (1) appears under reduced conditions, whereas (2) and (3) are seen when the disulfide bond is formed. In order to explain what force causes the transition from (1) to (2) and (3), we made a simple model by a rubber tube as shown in Fig. 14A. Because the two terminals of the rubber tube are connected to two stands, a loop is made. When the loop is pinched by moving the stands named 'N', the loop is turned over (Fig. 14C). When the movement of stand N is not large enough, the rubber loop is in the intermediate conformation with one side of the loop touching the ground and the other side far from the ground (Fig. 14B). Fig. 14A corresponds to state (1) of the GH loop, whereas Fig. 14B corresponds to state (3). In order to climb a barrier from state (1) to state (3), a transient and disturbed state (2) should appear. Considering this simple rubber tube model, the conformational transition of the GH loop is an inescapable consequence of pinching the loop by the disulfide bond. Thus the conformational transition is caused by elastic force and geometrical restrictions.

Although the centre of motion of the GH loop should be directed toward the 5-fold axis under unreduced conditions (yellow circle in Fig. 9A) as previously proposed (the conventional up state) [4], the loop was actually directed toward the 2-fold axis (2b in Fig. 1) in MD simulation (Fig. 9). The result is consistent with the data for X-ray structures of capsids of viruses including rhinovirus [41], poliovirus [42] and many other picornaviruses in which the GH loop of VP1 is ordered and directed approximately toward the 2-fold axis.

For the backbone conformation of the RGD tripeptide, the tripeptide has been reported as being more strongly kinked in ligands specific to αvβ3 than in those specific to αIIbβ3 [43,44].

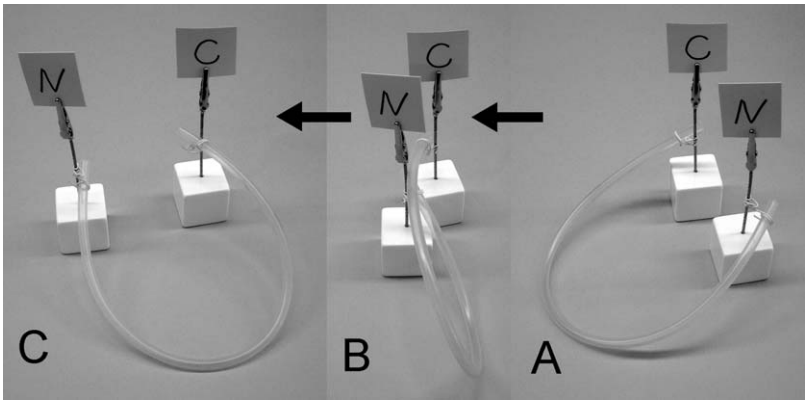

Fig. 14. Model of silicone rubber tube to explain conformational change of the GH loop. The two stands named 'N' and 'C' are put on the ground. The two terminals of the rubber tube are loosely connected to the stands. (A) Initially, the tube forms a loop. (C) When stand 'N' is moved toward left, the loop turns down and the direction of the loop is changes. (B) The intermediate state between A and C. Practically, the motion of the tube from A to C needs some assistance of human hands, because of gravity. However, when the bases of the stands are fixed on a vertical wall or the model is put in a water pool, the tube moves more automatically according to the motion of the stand.

However, opposition to this proposition has been reported [45]. Both the kink and extend conformations of the RGD tripeptide appeared in our MD simulation, but this appearance provides only marginal information for the debate. Furthermore, it has recently been suggested that the main receptor of the FMDV may be integrin αvβ6 [14,46].

The side chains of Arg145 and Asp147 extended in opposite directions (Fig. 12). This structure is not uncommon in other integrin ligands [14] or in the integrin–ligand complex [23]. Concerning the specificity to subtypes of integrins, some residues flanking the RGD tripeptide are known to be conserved across the different FMDV variants, and the leucine residues at the first and fourth sites following RGD (RGD+1 and RGD+4) (Leu148 and Leu151) can play a key role in binding of the GH loop to integrin αvβ6 [14,46]. Recently, experimental analysis has been performed by DiCara et al. on 20-mer peptides including the GH loop of FMDV serotype O [47]. They reported that the RGD tripeptide is followed by a C-terminal helix and that the hydrophobic residues at RGD+1 and RGD+4 are exposed almost in apposition on one face of the helix. They also reported that the potency to bind integrin αvβ6 is stronger for the peptide with longer and more stable helix and that the hydrophobic residues may be involved in the binding to integrin αvβ6. The results obtained from the present simulation support their results. The hydrophobic residues on the C-terminal side including Leu148 and Leu151 were driven by the hydrophobic force to form a cluster in the present simulation including the surrounding water. The cluster continued to be in close proximity of Asp147 except when the GH loop fluctuated like a tentacle. From physical view points, if the hydrophobic cluster is located near Asp147 when the RGD tripeptide is bound with integrin, the electrostatic interaction between Asp147 and a metal ion in the metal-ion-dependent adhesion site (MIDAS) of integrin would be enhanced, because the effective dielectric constant would be reduced by excluding water from the surrounding environment.

The present MD simulation using the RSBC method provided detailed information on the structure and dynamics of the GH loop of FMDV. Mechanism of uncoating and assembly of capsids can be also studied by further longer simulations.

References

[1] B.W.J. Mahy, in: B.W.J. Mahy (Ed.), Foot-and-mouth Disease Virus, Springer-Verlag, Berlin, 2005, pp. 1–8.
[2] E.E. Fry, D.I. Stuart, D.J. Rowland, in: B.W.J. Mahy (Ed.), Foot-and-mouth Disease Virus, Springer-Verlag, Berlin, 2005, pp. 71–101.
[3] R. Acharya, E. Fry, D. Stuart, G. Fox, D. Rowlands, F. Brown, Nature 337 (1989) 709.
[4] N. Parry, G. Fox, D. Rowlands, F. Brown, E. Fry, R. Acharya, D. Logan, D. Stuart, Nature 347 (1990) 569.
[5] D. Logan, R. Abu-Ghazaleh, W. Blakemore, S. Curry, T. Jackson, A. King, S. Lea, R. Lewis, J. Newman, N. Parry, D. Rowlands, D. Stuart, E. Fry, Nature 362 (1993) 566.
[6] E.E. Fry, S.M. Lea, T. Jackson, J.W.I. Newman, F.M. Ellard, W.E. Blakemore, R. Abu-Ghazaleh, A. Samuel, A.M.Q. King, D.I. Stuart, EMBO J. 18 (1999) 543.
[7] S. Lea, R. Abu-Ghazaleh, W. Blakemore, S. Curry, E. Fry, T. Jackson, A. King, D. Logan, J. Newman, D. Stuart, Structure 3 (1995) 571.
[8] S. Lea, J. Hernández, W. Blakemore, E. Brocchi, S. Curry, E. Domingo, E. Fry, R. Abu-Ghazaleh, A. King, J. Newman, D. Stuart, M.G. Mateu, Structure 2 (1994) 123.
[9] S. Curry, E. Fry, W. Blakemore, R. Abu-Ghazaleh, T. Jackson, A. King, S. Lea, J. Newman, D. Rowlands, D. Stuart, Structure 4 (1996) 135.
[10] E.E. Fry, J.W.I. Newman, S. Curry, S. Najjam, T. Jackson, W. Blakemore, S.M. Lea, L. Miller, A. Burman, A.M.Q. King, D.I. Stuart, J. Gen. Virol. 86 (2005) 1909.
[11] H.M. Berman, J. Westbrook, Z. Feng, G. Gilliland, T.N. Bhat, H. Weissig, I.N. Shindyalov, P.E. Bourne, Nucleic Acids Res. 28 (2000) 235.
[12] E. Fry, R. Acharya, D. Stuart, Acta Crystallogr. A 49 (1993) 45.
[13] R.O. Hynes, Cell 110 (2002) 673.
[14] J. Takagi, Curr. Opin. Cell Biol. 19 (2007) 557.
[15] N. Verdaguer, M.G. Mateu, D. Andreu, E. Giralt, E. Domingo, I. Fita, EMBO J. 14 (1995) 1690.
[16] N. Verdaguer, M.G. Mateu, J. Bravo, E. Domingo, I. Fita, J. Mol. Biol. 256 (1996) 364.
[17] N. Verdaguer, N. Sevilla, M.L. Valero, D. Stuart, E. Brocchi, D. Andreu, E. Giralt, E. Domingo, M.G. Mateu, I. Fita, J. Virol. 72 (1998) 739.
[18] W.F. Ochoa, S.G. Kalko, M.G. Mateu, P. Gomes, D. Andreu, E. Domingo, I. Fita, N. Verdaguer, J. Gen. Virol. 81 (2000) 1495.
[19] E.A. Hewat, N. Verdaguer, I. Fita, W. Blakemore, S. Brookes, A. King, J. Newman, E. Doming, M.G. Mateu, D.I. Stuart, EMBO J. 16 (1997) 1492.
[20] N. Verdaguer, G. Schoehn, W.F. Ochoa, I. Fita, S. Brookes, A. King, E. Domingo, M.G. Mateu, D. Stuart, E.A. Hewat, Virology 255 (1999) 260.
[21] J.-P. Xiong, T. Stehle, B. Diefenbach, R. Zhang, R. Dunker, D.L. Scott, A. Joachimiak, S.L. Goodman, M.A. Arnaout, Science 294 (2001) 339.
[22] T. Xiao, J. Takagi, B.S. Coller, J.-H. Wang, T.A. Springer, Nature 432 (2004) 59.
[23] J.-P. Xiong, T. Stehle, R. Zhang, A. Joachimiak, M. Frech, S.L. Goodman, M.A. Arnaout, Science 296 (2002) 151.
[24] T. Cagin, M. Holder, B.M. Pettitt, J. Comput. Chem. 12 (1991) 627.
[25] S. Yoneda, M. Kitazawa, H. Umeyama, J. Comput. Chem. 17 (1996) 191.
[26] D.K. Phelps, B. Speelman, C.B. Post, Curr. Opin. Struct. Biol. 10 (2000) 170.
[27] P.L. Freddolino, A.S. Arkhipov, S.B. Larson, A. McPherson, K. Schulten, Structure 14 (2006) 437.
[28] S. Yoneda, T. Yoneda, Y. Kurihara, H. Umeyama, J. Mol. Graph. Model. 21 (2002) 19.
[29] T. Yoneda, S. Yoneda, N. Takayama, M. Kitazawa, H. Umeyama, J. Mol. Graph. Model. 17 (1999) 114.
[30] S. Yoneda, J. Mol. Graph. Model. 15 (1997) 233.
[31] U.C. Singh, F.K. Brown, P.A. Bash, P.A. Kollman, J. Am. Chem. Soc. 109 (1987) 1607.
[32] S. Yoneda, H. Umeyama, J. Chem. Phys. 97 (1992) 6730.
[33] W.D. Cornell, P. Cieplak, C.L. Bayly, I.R. Gould, K.M. Merz Jr., D.M. Ferguson, D.C. Spellmeyer, T. Fox, J.W. Caldwell, P.A. Kollman, J. Am. Chem. Soc. 117 (1995) 5179.
[34] Y. Duan, C. Wu, S. Chowdhury, M.C. Lee, G. Xion, W. Zhang, R. Yang, P. Cieplak, R. Luo, T. Lee, J. Caldwell, J. Wang, P. Kollman, J. Comput. Chem. 24 (2003) 1999.
[35] W.L. Jorgensen, J. Chandrasekhar, J.D.R. Madura, R.W. Impey, M.L. Klein, J. Chem. Phys. 79 (1983) 926.
[36] M.P. Allen, D.J. Tildesley, Computer Simulations of Liquids, Oxford University Press, New York, 1987.
[37] J.-P. Ryckaert, G. Cicotti, H.J.C. Berendsen, J. Comput. Phys. 23 (1977) 327.
[38] H.J.C. Berendsen, J.P.M. Postma, W.F. van Gunsteren, A. DiNola, J.R. Haak, J. Chem. Phys. 81 (1984) 3684.
[39] W. Kabsch, C. Sander, Biopolymers 22 (1983) 2577.

[40] T. Schwede, J. Kopp, N. Guex, M.C. Peitsch, Nucleic Acids Res. 31 (2003) 3381.
[41] M.G. Rossmann, E. Arnold, J.W. Erickson, E.A. Frankenberger, J.P. Griffith, H.J. Hecht, J.E. Johnson, G. Kamer, M. Luo, A.G. Mosser, R.R. Rueckert, B. Sherry, G. Vriend, Nature 317 (1985) 145.
[42] D.J. Filman, R. Syed, M. Chow, A.J. Macadam, P.D. Minor, J.M. Hogle, EMBO J. 8 (1989) 1567.
[43] R. Haubner, R. Gratias, B. Diefenbach, S.L. Goodman, A. Jonczyk, H. Kessler, J. Am. Chem. Soc. 118 (1996) 7461.
[44] D. Heckmann, H. Kessler, Meth. Enzymol. 426 (2007) 463.
[45] L. Belvisi, A. Bernardi, M. Colombo, L. Manzoni, D. Potenza, C. Scolastico, G. Giannini, M. Marcellini, T. Riccioni, M. Castorina, P. LoGiudice, C. Pisano, Bioorg. Med. Chem. 14 (2006) 169.
[46] A. Burman, S. Clark, N.G.A. Abrescia, E.E. Fry, D.I. Stuart, T. Jackson, J. Virol. 80 (2006) 9798.
[47] D. DiCara, C. Rapisarda, J.L. Sutcliffe, S.M. Violette, P.H. Weinreb, I.R. Hart, M.J. Howard, J.F. Marshall, J. Biol. Chem. 282 (2007) 9657.